Effect of thin silicon dioxide layers on resonant frequency in infrared metamaterials

D. J. Shelton[1,*], D. W. Peters[2], M. B. Sinclair[2], I. Brener[2], L. K. Warne[2], L. I. Basilio[2], K. R. Coffey[3], and G. D. Boreman[1,3]

[1]*CREOL, University of Central Florida, 4000 Central Florida Blvd., Orlando FL 32816-2700, U.S.A.*
[2]*Sandia National Laboratories, P.O. 5800, Albuquerque NM 87185-1082, U.S.A.*
[3]*AMPAC, University of Central Florida, 4000 Central Florida Blvd., Orlando FL 32816-2700, U.S.A.*
**dshelton@creol.ucf.edu*

Abstract: Infrared metamaterials fabricated on semiconductor substrates exhibit a high degree of sensitivity to very thin (as small as 2 nm) layers of low permittivity materials between the metallic elements and the underlying substrate. We have measured the resonant frequencies of split ring resonators and square loops fabricated on Si wafers with silicon dioxide thicknesses ranging from 0 to 10 nm. Resonance features blue shift with increasing silicon dioxide thickness. These effects are explained by the silicon dioxide layer forming a series capacitance to the fringing field across the elements. Resonance coupling to the Si-O vibrational absorption has been observed. Native oxide layers which are normally ignored in numerical simulations of metamaterials must be accounted for to produce accurate predictions.

OCIS codes: (160.3918) Metamaterials; (300.6340) Spectroscopy, infrared.

References and links

1. D. Shelton, J. Ginn, and G. Boreman, "Bandwidth variations in conformal infrared frequency selective surfaces," IEEE Antennas Propag. International Symposium, 3976 (2007)
2. D. H. Kwon, X. Wang, Z. Bayraktar, B. Weiner, and D. H. Werner, "Near-infrared metamaterial films with reconfigurable transmissive/reflective properties," Opt. Lett. **33**(6), 545–547 (2008).
3. B. Kanté, A. de Lustrac, and J. M. Lourtioz, "In-plane coupling and field enhancement in infrared metamaterial surfaces," Phys. Rev. B **80**(3), 035108 (2009).
4. J. Ginn, D. Shelton, P. Krenz, B. Lail, and G. Boreman, "Altering infrared metamaterial performance through metal resonance damping," J. Appl. Phys. **105**(7), 074304 (2009).
5. B. Monacelli, J. Pryor, B. A. Munk, D. Kotter, and G. Boreman, "Infrared frequency selective surface based on circuit-analog square loop design," IEEE Trans. Antenn. Propag. **53**(2), 745–752 (2005).
6. J. F. O'Hara, E. Smirnova, H. T. Chen, A. J. Taylor, R. D. Averitt, C. Highstrete, M. Lee, and W. J. Padilla, "Properties of planar electric metamaterials for novel terahertz applications," J. Nanoelectron. Optoelectron. **2**(1), 90–95 (2007).
7. N. I. Landy, S. Sajuyigbe, J. J. Mock, D. R. Smith, and W. J. Padilla, "Perfect metamaterial absorber," Phys. Rev. Lett. **100**(20), 207402 (2008).
8. J. Ginn, B. Lail, J. Alda, and G. Boreman, "Planar infrared binary phase reflectarray," Opt. Lett. **33**(8), 779–781 (2008).
9. J. Tharp, B. Lail, B. Munk, and G. Boreman, "Design and demonstration of an infrared meanderline phase retarder," IEEE Trans. Antenn. Propag. **55**(11), 2983–2988 (2007).
10. E. Cubukcu, S. Zhang, Y. S. Park, G. Bartal, and X. Zhang, "Split ring resonator sensors for infrared detection of single molecular monolayers," Appl. Phys. Lett. **95**(4), 043113 (2009).
11. B. Kanté, A. de Lustrac, J. M. Lourtioz, and F. Gadot, "Engineering resonances in infrared metamaterials," Opt. Express **16**(10), 6774–6784 (2008), http://www.opticsinfobase.org/abstract.cfm?URI=oe-16-10-6774.
12. W. J. Padilla, A. J. Taylor, C. Highstrete, M. Lee, and R. D. Averitt, "Dynamical electric and magnetic metamaterial response at terahertz frequencies," Phys. Rev. Lett. **96**(10), 107401 (2006).
13. D. Li, Y. J. Xie, P. Wang, and R. Yang, "Applications of Split-ring resonances on multi-band frequency selective surfaces," J. Electromagn. Waves Appl. **21**(11), 1551–1563 (2007).
14. H. Leplan, B. Geenen, J. Y. Robic, and Y. Pauleau, "Redidual stresses in evaporated silicon dioxide thin films: Correlation with deposition parameters and aging behavior," J. Appl. Phys. **78**(2), 962 (1995).
15. N. M. Sushkova, and A. G. Akimov, "Formation of 3D islands of metal oxides on silicon covered by native oxide film by multi-step ion sputtering of Ti, Nb and V," Vacuum **56**(4), 287–291 (2000).
16. D. J. Shelton, T. Sun, J. C. Ginn, K. R. Coffey, and G. D. Boreman, "Relaxation time effects on dynamic conductivity of alloyed metallic thin films in the infrared band," J. Appl. Phys. **104**(10), 103514 (2008).
17. M. G. Moharam, and T. K. Gaylord, "Rigorous coupled-wave analysis of planar-grating diffraction," J. Opt. Soc. Am. **71**(7), 811 (1981).

#120207 - $15.00 USD Received 20 Nov 2009; revised 22 Dec 2009; accepted 23 Dec 2009; published 7 Jan 2010

1. Introduction

Metamaterials have been fabricated for infrared (IR) systems to control spectral reflection [1,2], transmission [3,4], emission [5,6], absorption [7], reflected phase [8], as broad-band wave plates [9], and for molecular detection [10]. These devices were built on Si wafers, and the impact of the native oxide layer on device performance has not been studied to date. It is reasonable to expect that such layers will have an effect, since the resonance of metallic IR metamaterial elements will be impacted by their fringing-field capacitance which results from intra-element fields between opposite sides of the element. These fields pass through the interface between the metal elements and the Si wafer; when a native oxide or other thin insulating layer is present this capacitance may change considerably.

This paper demonstrates the sensitivity of IR metamaterials fabricated on semiconductor substrates to thin silicon dioxide (SiO_2) layers. This sensitivity is manifest as an SiO_2-thickness-dependent shift in the spectral location of both resonances as well as coupling between the SRR resonance and the Si-O absorption resonance. The native oxide effect explains blue shifting in the resonance spectral location in measurements compared to numerical simulations that is commonly seen in the literature such as Ref. 11.

2. Theory

Split-ring resonator (SRR) type metamaterials operating near 1 THz exhibit dual resonances when incident radiation is linearly polarized parallel to the gap in the elements [12]. By scaling down the size of the SRR elements dual resonances in the IR at wavelengths of 4 and 10 μm (75 and 30 THz) may be achieved. A schematic of an SRR element with labeled dimensions is given in Fig. 1.

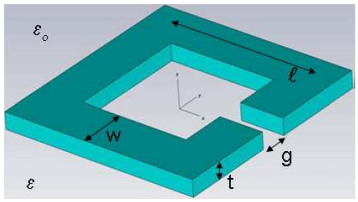

Fig. 1. (Color online) Schematic of SRR element.

The high frequency resonance at 4 μm is due to coupling between elements in the array and is described in Ref. 13. The fundamental resonance at 10 μm is due to the electronic resonance of the unit cell and may be described as an RLC circuit with resonance frequency, ω_0, as defined by Eq. (1).

$$\omega_0 = \frac{1}{(LC)^{1/2}} = \frac{1}{\left[L\left(C_g + C_f\right)\right]^{1/2}} \tag{1}$$

For SRRs C_g is the gap capacitance defined by Eq. (2) with permittivity of free space ε_0.

$$C_g = \varepsilon_0 \left(\frac{wt}{g}\right) \tag{2}$$

The TiO_2 layers that occur as part of the adhesion layer and the SiO_2 layer beneath the elements form a series capacitance to the fringing field across the diameter of the SRR. This fringing-field capacitance, C_f, depends upon the permittivity and thickness of the thin film stack of lower index oxide layers that exist between the SRR elements and the Si substrate as shown schematically in Fig. 2.

#120207 - $15.00 USD Received 20 Nov 2009; revised 22 Dec 2009; accepted 23 Dec 2009; published 7 Jan 2010

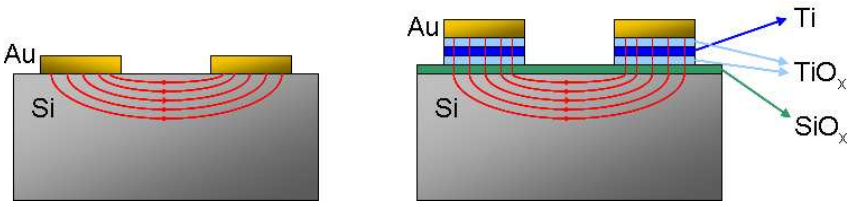

Fig. 2. (Color online) Schematic of fringing-field capacitance where electric field lines are shown across the diameter of the SRR penetrating the oxide layers beneath the elements.

As the thickness of the SiO_2 layer, t_{SiO2}, increases relative to the penetration depth of the resonant electric field mode, t_n, C_f decreases according to Eq. (3)

$$C_f = \left[\varepsilon_0 + \varepsilon_{SiO2}\left(1 - \frac{t_{SiO2}}{t_n}\right) + \varepsilon_{TiO2}\left(1 - \frac{t_{TiO2}}{t_n}\right) \right] \times \eta \tag{3}$$

where ε_{SiO2} and ε_{TiO2} are permittivities of SiO_2 and TiO_2 respectively. The term η is a geometrical factor given by Eq. (4).

$$\eta = \frac{\pi \ell}{3\ln(\ell / a)} + \frac{(2w + 2t)}{2\pi}\left[\ln\left(\frac{4a}{g}\right) - \gamma - \frac{2}{15} \right] \tag{4}$$

In Eq. (4) a is the rectangular equivalent radius to a circular loop and γ is Euler's constant. The inductance may be computed based on the geometry using Eq. (5).

$$L = \frac{\mu_0}{\pi}(2\ell)\left[\ln\left(\frac{\ell}{a}\right) - \gamma + \frac{a}{\ell} \right] \tag{5}$$

By combining Eqs. (1) and 3 it is clear that as the thickness of the SiO_2 layer increases the reduction in the fringing-field capacitance will decrease resulting in a blue-shifting effect on the resonant frequency of the metamaterial. Since a similar fringing-field effect may be expected to occur between elements, it should also be the case that a blue shift should be observed in the high frequency resonance as the SiO_2 thickness increases.

3. Experiment and fabrication

An experiment was designed to test the effect of thin SiO_2 layers from 0 to 10 nm thick at the interface between the elements and the Si substrate. For 0 nm SiO_2 thickness a hydrogen terminated Si surface was used. A 2 nm SiO_2 thickness was achieved using the native oxide on the Si wafer. Further 2 nm increments in SiO_2 thickness up to 10 nm were produced by depositing SiO_2 onto Si wafers, taking into account the native oxide layer. This was done by electron-beam evaporation using *in situ* ellipsometry to monitor the SiO_2 thickness. A J.A. Woolam M-2000 ellipsometer was used for both the native oxide and *in situ* thickness measurements. Evaporated SiO_2 films have been found to have the correct stoichiometry [14], but a density that is reduced relative to thermally grown films. A single layer of SRR and square-loop elements was fabricated on these wafers using electron-beam lithography. The SRR elements (see the inset of Fig. 4) had a 1 μm periodicity, 750 nm lengths, 150 nm arm widths, and a 120 nm gaps. The square-loop (see the inset of Fig. 5) had a 2.23 μm periodicity, 1650 nm length, and a 300 nm arm width. For the 0 nm SiO_2 sample the resist pattern was exposed to dilute HF for 30 s to produce a hydrogen terminated surface before metallization. Then, a 5 nm adhesion layer of Ti was deposited onto the resist patterned wafer, followed by 75 nm of Au. The metals were deposited by electron-beam evaporation at a base pressure of 5×10^{-6} Torr, and a lift-off process was used to produce the elements.

About 5 minutes elapsed between the Ti and Au depositions as the source was changed. During that time some of the Ti seed layer was converted to TiO_2 by the absorption of residual oxygen in the chamber [15]. The Ti seed layer appears at the location of highly localized surface plasmon oscillations between the Au elements and the Si substrate, and thus the inclusion of accurate spectral permittivity values in simulations for both TiO_2 and evaporated SiO_2 layers is critical to produce good agreement between simulation and

#120207 - $15.00 USD Received 20 Nov 2009; revised 22 Dec 2009; accepted 23 Dec 2009; published 7 Jan 2010

measurement. The IR optical constants for Ti, TiO_2, and SiO_2 were measured on 100 nm thick evaporated films using a J.A. Wollam IR VASE ellipsometer. Figure 3 shows the results of these measurements. The IR optical constants for Au films have been discussed in Ref. 16.

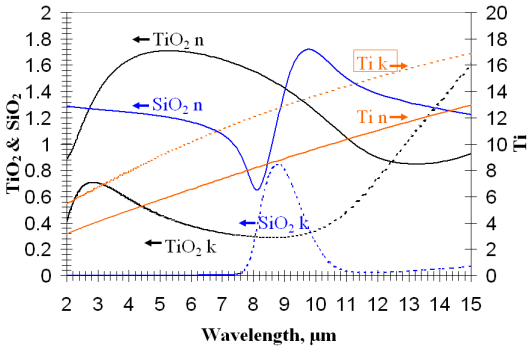

Fig. 3. (Color online) IR optical constants for evaporated SiO_2, TiO_2, and Ti measured using IR VASE system.

4. Results

Simulations of the spectral transmission of the SRR structures with thin SiO_2 layers were performed using rigorous coupled wave analysis (RCWA) [17] incorporating the measured optical constants shown in Fig. 3. The spectral transmission was measured using FTIR with the incident radiation linearly polarized parallel to the gap in the elements. Figures 4-5 show the measured and simulated results for an incremental increase in the SiO_2 thickness from 0 to 10 nm. The FTIR measurements with SiO_2 layers 4 nm and thicker are noiser than the 0 and 2 nm thick measurements due to the likely presence of voids in the thin evaporated SiO_2 layers. However the noise does not obscure the blue shift in the resonant frequency.

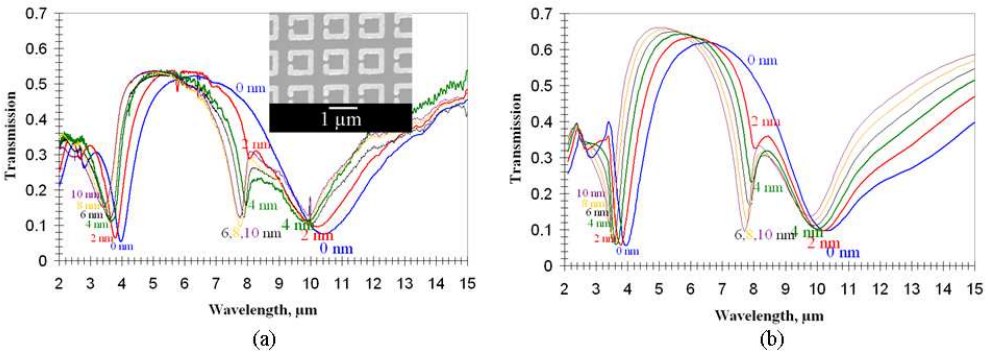

Fig. 4. (color online) FTIR measurements of SRR metamaterials with SiO_2 layer thickness indicated and SEM insert of fabricated elements in (a), RCWA simulations of same structures shown in (b).

#120207 - $15.00 USD Received 20 Nov 2009; revised 22 Dec 2009; accepted 23 Dec 2009; published 7 Jan 2010

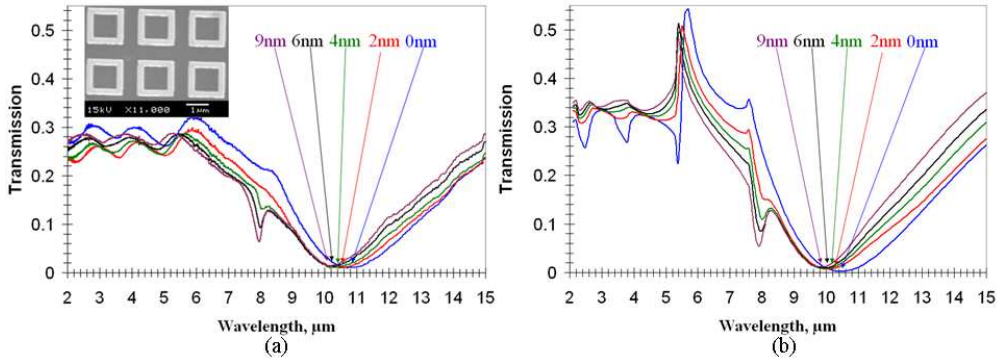

Fig. 5. (color online) FTIR measurements of square-loop metamaterials with SiO_2 layer thickness indicated and SEM insert of fabricated elements in (a), RCWA simulations of same structures shown in (b).

The RCWA simulation accurately reproduces the FTIR measurements when the Ti seed layer is treated as a three-layer stack consisting of 1.25 nm of TiO_2, 2.5 nm of Ti, and 1.25 nm of TiO_2 to account for the oxidation in the vacuum chamber. Some discrepancy between the magnitude in the FTIR measurements and the RCWA simulations occurred because back-side wafer reflections were not included in the RCWA modeling.

The measured long wavelength resonance at 10 μm shifts to shorter wavelengths as the SiO_2 thickness increases, with the shift slowing for incremental additions over 4 nm. The SRR short wavelength resonance displayed similar behavior as the long wavelength resonance, except the resonance continues to shift for thicker SiO_2 layers. Furthermore, a transmission minimum is observed near 8 μm that is related to absorption due to coupling between the SRR or square-loop resonance and the Si-O vibrational band in the SiO_2 layer. At zero-SiO_2-thickness this minimum is not observed in either element type.

5. Discussion

Using Eqs. (1-4) the fringing-field capacitance model may be compared to the FTIR and RCWA results for the SRRs. Based on the dimensions of the SRRs the impedance, L, was calculated to be 0.74 pH, the gap capacitance, C_g, was 0.83 aF, and the fringing-field capacitance, C_f, was 40.1 aF for zero SiO_2 thickness. To calculate the expected change in the resonant frequency based upon C_f as the SiO_2 thickness increased we considered that t_n was approximately equal to 60 nm. The analytical results are compared to the FTIR measurements and RCWA simulations in Table 1.

Table 1. Comparison of fundamental resonant frequency measured by FTIR to simulation and analytical calculations.

SiO_2 thickness (nm)	FTIR $\lambda_{0,1}$ (μm)	RCWA $\lambda_{0,1}$ (μm)	Analytical $\lambda_{0,1}$ (μm)
0	10.42	10.35	10.4
2	10.21	10.15	10.2
4	9.94	10.02	10.0
6	10.00	9.91	9.85
8	9.93	9.84	9.67
10	9.95	9.76	9.49

The most significant discrepancy between the measured and analytical results occurs as the SiO_2 thickness increases from 4 to 10 nm. This is due to strong coupling between the SRR resonance and the Si-O vibrational absorption. When the two resonances are coupled their resonant frequencies repel each other resulting in a red shift to the measured resonance that is not accounted for in the current analytical model.

#120207 - $15.00 USD Received 20 Nov 2009; revised 22 Dec 2009; accepted 23 Dec 2009; published 7 Jan 2010

As seen in Figs. 4-5, the SRR shows a stronger coupling to the Si-O absorption than the square-loop. The Si-O absorption near 8 μm is not visible in FTIR scans of unpatterned SiO_2 films with thicknesses ranging between 0 and 10 nm, indicating that the appearance of this feature in the metamaterial films arises due to resonant enhancement. Additionally in the zero SiO_2 thickness measurement in Figs. 4-5 only the area beneath the elements was hydrogen terminated, and thus a native oxide layer surrounded the elements. The absence of an effect for this sample indicates that only the element to substrate interface is responsible for the sensitivity to thin SiO_2 layers.

Figure 6 compares the on-resonance electric field intensity, obtained using finite-element method Ansoft HFSS software [18], at the interface between the metallic elements and the SiO_2 layer of a square-loop element as in Ref. 5 to a split-ring element. Both element types are scaled to resonate at 30 THz with similar bandwidths when arrayed with a unit-cell spacing which is 1.4 times the length of the element. In both simulations the electric field was a TM mode polarized in the direction perpendicular to the gap of the SRR in Fig. 6. The smaller dimensions and narrow gap of the split ring results in a maximum electric field magnitude of 1.5×10^9 V/m compared to 1×10^8 V/m in the square ring. As seen by comparing the absorption dip at 8 μm in Figs. 4 and 5, the SRR showed more sensitivity to coupling to the Si-O absorption band than the square-loop, and thus we conclude that the stronger electric field at the surface of the SRR element leads to more resonantly enhanced absorption in the adjacent SiO_2 layer.

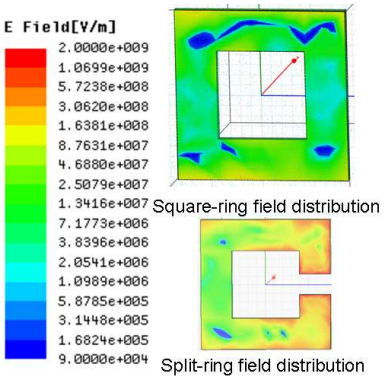

Fig. 6. (color online) Electric field intensity calculated by finite-element method HFSS simulation at element to substrate interface for square ring compared to SRR element from Ref. 5.

6. Conclusion

In conclusion, SRR resonances exhibit sensitivity to a very thin (as small as 2nm) layer of native oxide present on a Si wafer due to adding a series capacitance to the fringing-field capacitance. The spectral locations of resonance features shift to shorter wavelength as the SiO_2 layer located between the Si substrate and the metallic elements increases in thickness from 0 to 10 nm. The spectral shifting is similar for both square-loop and SRR elements, and thus it does not depend greatly on the fringing-field strength or on the presence of a gap. Coupling between the SRR resonance and SiO_2 absorption band was also observed to result in an additional resonance feature, whose strength is dependent on the electric field strength immediately below the metallic element, and may be useful in a sensor application to enhance detection. The thin-SiO_2 resonance shift is an important design consideration for all metamaterial structures on high-index substrates with native oxide layers present.

Acknowledgements

This research was supported by the Laboratory Directed Research and Development program at Sandia National Laboratories. Sandia is a multiprogram laboratory operated by Sandia Corporation, a Lockheed Martin Company, for the United States Department of Energy's National Nuclear Security Administration under Contract DE-AC04-94AL85000.